Persistent spectral hole burning for R' color centers in LiF crystals: Statics, dynamics, and external-field effects

W. E. Moerner, P. Pokrowsky,* F. M. Schellenberg, and G. C. Bjorklund
IBM Almaden Research Center, San Jose, California 95120-6099
(Received 22 November 1985)

The persistent spectral hole-burning properties of R' color centers in pure and doped LiF single crystals at liquid-helium temperatures are described and analyzed. Using frequency-modulation spectroscopy and precision ratiometric transmission spectroscopy, a satellite hole structure has been observed which varies with position in the inhomogeneous line due to excited-state splittings. Transient effects in the optical absorption indicate that an intermediate state with millisecond lifetimes is involved in hole formation. The persistent holes have been observed to grow as the logarithm of time and the logarithm of burning intensity in certain regimes, and a phenomenological tunneling model has been used to explain the time and intensity dependence. The results suggest that R' centers interact via tunneling and local strains with a quasi-random distribution of nearby traps which may be other color centers in the host material. A linear Stark effect has been observed in agreement with earlier measurements. This work illustrates the power of hole-burning spectroscopy to uncover static and dynamic interactions normally hidden by inhomogeneous broadening.

I. INTRODUCTION

Persistent spectral hole burning (PHB) has been demonstrated to be an important method for studying basic properties of absorbing centers in solids that can be phototransformed between several possible ground states at liquid-helium temperatures.[1,2] The mechanisms leading to persistent spectral holes (i.e., those with lifetimes longer than any excited-state lifetime) have been classified as being either photochemical, in which the center itself undergoes photoionization, tautomerization, or some other chemical reaction,[3] or photophysical (also termed nonphotochemical),[4,5] in which the photoinduced shift in absorption occurs due to reorientation of the center itself or to rearrangement of the nearby host. In addition, persistent spectral hole burning forms the basis for a possible new optical-storage scheme, frequency-domain optical storage,[6,7] in which spectral holes in an inhomogeneously broadened absorption profile at low temperatures are used to encode digital information. Consequently, the properties of absorbing centers that show persistent spectral hole production are of interest in both the scientific and technological communities.

Aggregate color centers in ionic solids provide a large number of inhomogeneously broadened zero-phonon-line (ZPL) optical transitions that may be studied for PHB.[8] Early in the history of hole burning, several color centers in x-irradiated NaF were shown to undergo phototransformation at low temperatures, resulting in the formation of persistent spectral holes.[9,10] The mechanism of hole formation in these systems has been postulated to be photochemical, involving photoinduced tunneling of the excited electron away from the color center to a nearby trap. Recently, contrary to the low (10^{-6}) quantum efficiencies observed for most color centers,[2,9,10] high- (10^{-2}) efficiency PHB was reported for the F_4^- aggregate center in electron-irradiated NaF:OH^-.[11]

In this work we study the process of persistent spectral hole formation for the 8330-Å ZPL corresponding to R' (or F_3^-) color centers in pure (natural as well as isotopically enriched) LiF crystals as well as in LiF crystals with several secondary dopants. The center consists of three anion vacancies arranged in an equilateral triangle in the (111) plane trapping four electrons. The zero-phonon absorption of this center was initially discovered and studied using monochromator-resolution spectroscopy of the entire inhomogeneous line.[12–14] Here we use the high-resolution technique of spectral hole burning to probe the properties of the center inside the inhomogeneously broadened absorption profile. This system was the first material to show PHB in the technologically important GaAlAs laser-wavelength region (7500–8500 Å) as demonstrated with an infrared dye laser[15] and later with semiconductor diode lasers.[16] Recent experiments have reported near-infrared hole burning in the 8892-Å center in NaF:OH^- (Ref. 11) and in organic materials as well.[17] The hole-erasing properties of the R' center in polycrystalline thin films of LiF have been reported elsewhere.[18] The hole line-shape systematics for dopants and coloration methods other than those studied here are the subject of recent work.[19]

This paper presents a summary of the statics, dynamics, and response to dc electric and magnetic fields of spectral holes for R' centers in pure and doped LiF single crystals. Using both laser frequency-modulation (FM) spectroscopy[20] and ratiometric transmission spectroscopy, we have determined the low-power hole width at 1.3 K, the variation in hole shape as a function of position within the inhomogeneous line, the hole-growth kinetics including quantum efficiency, the effects of several dopants, and the Stark and Zeeman effects. Using a simple tunneling model, we suggest microscopic origins for the logarithmic hole-growth characteristic. The results presented here clearly show the power of PHB spectroscopy in uncover-

ing static and dynamic interactions in solids normally hidden by the inhomogeneously broadened line. In the rest of this paper we describe these measurements in detail, in the hope that some of the unusual properties of this system will stimulate theoretical interest in the electron-tunneling and -trapping process thought to be responsible for hole formation in color centers as well as in PHB dynamics in general.

II. EXPERIMENTAL DETAILS

A. Samples

The samples used in this study were cleaved from Czochralski-grown[21] single-crystal boules of LiF that were in most cases intentionally doped by the addition of various dopants directly to the melt. Table I (first column) lists the compositions of the various samples where the concentrations listed refer to the amount of the dopant added. The actual concentrations of the dopant ions in the grown crystals were typically 10 times smaller. The bulk of the measurements were performed on crystals doped with Mg^{2+} ions in the form of MgF_2. (The divalent impurity is thought to stabilize the formation of the R' electron-excess center by removing free holes during irradiation and subsequent aggregation.[22]) Doping with CaF_2 and CuF_2 was also performed to test the effect of other divalent metal impurities. In addition, pure (natural) LiF obtained from Optovac, Inc. was utilized to test if the effects observed depended upon the presence of divalent dopant ions in the host. ^{6}LiF was obtained from Harshaw Chemical Company in the form of samples intended for thermoluminescent dosimetry (TLD) and therefore contained unknown proprietary secondary dopants. Pure ^{7}LiF was obtained from Harshaw Chemical Company in an already colored form by γ irradiation. All the other samples were colored by Cu or Mo $K\alpha$ x irradiation for 48—100 h at room temperature in a 850-W x-ray-diffraction machine, which initially yielded ZPL's with 50—75% absorptions that decayed to a depth of 20—50% after several days. For LiF doped with divalent impurities, after the initial decay no degradation of ZPL depth was observed on the time scale of 6 months or more.

Figure 1 shows a typical transmission spectrum of the R' ZPL for LiF + 0.05 mol% MgF_2 at 1.4 K obtained with the use of a Spex 0.75-m monochromator with 25-μm slits. Using a Burleigh WA-10 wavemeter and a single-frequency dye laser for calibration of the monochromator, we find the line center (vacuum wavelength) to be 8330.2±0.1 Å with a full width at half maximum (FWHM) absorption of 4.2±0.1 Å. All hole-burning measurements were performed at various locations within the corresponding inhomogeneously broadened ZPL for each sample. The phonon sideband at shorter wavelengths is not shown in this figure.

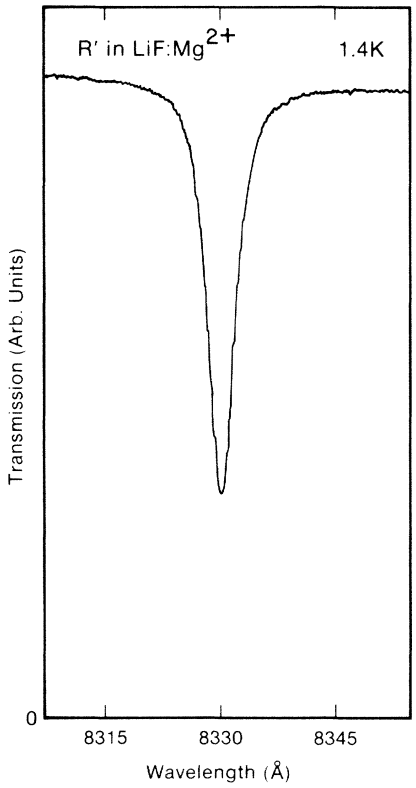

FIG. 1. Transmission spectrum of x-irradiated LiF + 0.05 mol% MgF_2, showing the R' zero-phonon-line absorption profile at 1.4 K.

TABLE I. R' ZPL properties for various host crystals.

Host	ZPL line center (Å)[a]	ZPL width (FWHM) (Å)[a]
LiF + 0.05 mol% MgF_2	8330.2	4.2
LiF + 0.2 mol% MgF_2	8331.2	6.5
LiF (pure, natural)	8330.1	4.3
LiF + 0.2 mol% CaF_2	8330.8	4.2
LiF + 0.2 mol% CuF_2	8331.5	5.1
^{6}LiF (TLD)	8335.4	7.2
^{7}LiF (TLD)	8330.5	7.4
^{7}LiF	8330.6	3.9

[a]Vacuum wavelength, accuracy: ±0.1 Å

Table I, second and third columns, summarizes the measured ZPL center wavelengths and widths for all the crystals used. The position of the ZPL can increase by as much as 1 Å due to the larger ionic radius of the Mg^{2+}, Ca^{2+}, and Cu^{2+} dopants. In addition, large concentrations of Mg^{2+} ions apparently increase the inhomogeneous broadening as measured by the ZPL width. The ^{6}LiF (TLD) sample shows an appreciable shift to longer wavelengths, reflecting the larger lattice constant of this host, in agreement with previously published results.[8] ^{7}LiF is similar to natural LiF owing to the 92.5% abundance of ^{7}Li in the natural material. The proprietary dopants in both TLD crystals are probably responsible for the larger ZPL linewidths in these hosts.

The hole-burning experiments were performed on samples either immersed in superfluid He at 1.4 K or maintained at a fixed temperature by flowing He boiloff gas

from a liquid-helium reservoir. Temperatures were measured with a calibrated carbon resistor.

B. Precision ratiometric transmission detection

Hole burning and hole detection were most often performed in transmission in order to detect the hole shape and amplitude directly. This dc-coupled method has several advantages. It is sensitive to slowly varying regions of the hole spectra and baseline shifts, and it is relatively easy to calibrate absolute absorption changes. However, sharp features are not particularly emphasized. The detailed experimental setup for precision ratiometric hole detection at low scanning laser powers has been described elsewhere.[11] Briefly, single-frequency laser radiation was provided by a 3-Mhz-linewidth Coherent 599-21 infrared dye laser (using Exciton Chemical Company LDS-820 or LDS-821 infrared-laser dye) pumped with 6471-Å radiation from a Spectra-Physics 171 Kr^+-ion laser. The laser beam was split into two beams: sample and reference. The sample beam was controlled by a mechanical shutter, attenuated with neutral-density filters, and focused to a 2.6-mm-diam spot at the sample. The holes were detected by attenuating the laser by 10^4, scanning the wavelength, and measuring the transmitted sample-beam power with a high-sensitivity silicon photodiode—low-noise preamplifier combination. Laser-power variations were removed from the transmission spectra by dividing the signal from the sample-beam preamplifier by the instantaneous laser power in the reference beam measured with a second silicon photodiode. The precision ratiometer typically had a 1-ms time constant. The resulting normalized transmission spectrum was offset and averaged typically 8 times with a digital storage oscilloscope. All frequency axes were calibrated by measuring the transmission of a 1.50-GHz free-spectral-range étalon. For the hole-growth measurements, the laser frequency was held fixed and the time-varying output of the ratiometer was digitized and stored without averaging.

C. Laser FM spectroscopy detection

For several experiments, laser FM spectroscopy was used for hole detection. Laser FM spectroscopy[20] is a zero-background technique particularly suited to high-speed measurement of sharp, weak absorptions and dispersions; however, this method is insensitive to broad features and baseline shifts and it is sometimes difficult to calibrate absolute absorption changes. The basic apparatus is shown in Fig. 2. Tunable single-frequency laser radiation at ω_c was provided by the infrared dye laser described above. A Lasermetrics 1097 $LiTaO_3$ electro-optic phase modulator driven at $\omega_m = 246$ MHz placed two out-of-phase sidebands on the laser carrier at $\omega_c \pm \omega_m$. After propagation through the sample, the laser carrier and sidebands were detected with a high-speed EG&G FND-100 photodiode. Any disturbance in the amplitude or phase of the sidebands due to frequency-dependent absorption or dispersion features (such as spectral holes) produced a beat signal at ω_m at the photodiode output. The photodiode signal was amplified, phase-shifted to select the absorption phase, bandpass-filtered at 246 MHz to reduce intermodulation products (not shown), and detected using a phase-sensitive double-balanced rf mixer driven at the local-oscillator (LO) frequency ω_m. The dc output of the mixer is proportional to the difference in optical absorption of the two sidebands, which yields a derivative line shape for absorption features wider than the sideband spacing. The mixer output was low-pass-filtered to remove signals not at baseband and amplified with a low-noise post-mixer preamplifier[23] (not shown) before display and averaging on a digital storage oscilloscope. For more details regarding the laser FM spectroscopy technique, the reader is referred to Refs. 20 and 24.

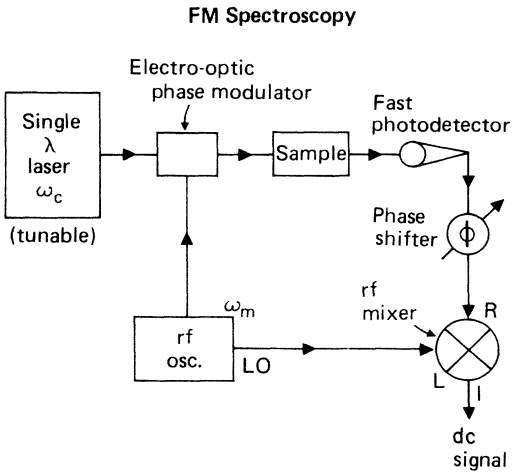

FIG. 2. Schematic of experimental apparatus for laser FM spectroscopy. The various components are described in the text.

III. RESULTS AND DISCUSSION

A. Statics of the persistent hole line shape: Side holes

1. Dependence upon position within the inhomogeneous line

As opposed to all other color centers in alkali halides in which PHB has been observed, the hole shape for R' centers in LiF varies with position within the inhomogeneous ZPL absorption. Figure 3 shows a sequence of holes burned at widely varying locations in the inhomogeneous line for a typical host material, LiF + 0.2 mol % MgF_2. These spectra were acquired using the ratiometric transmission methods described in Sec. II B above. Many more holes were burned at other locations within the ZPL, but these traces serve as a sampling of hole shapes that can be observed. For each trace, the narrow-band infrared dye laser was held at a different fixed wavelength labeled as 0 GHz in the figure. For this particular host, the ZPL line center was measured (by reference to the wavemeter) to be at 8331.2 Å. In the short-wavelength tail of the ZPL, a broad, almost featureless hole was observed, and traces (a) and (b) in Fig. 3 are typical of this region. Over a several Å region near the center of the ZPL, hole shapes like trace (c) were common. In the long-wavelength tail

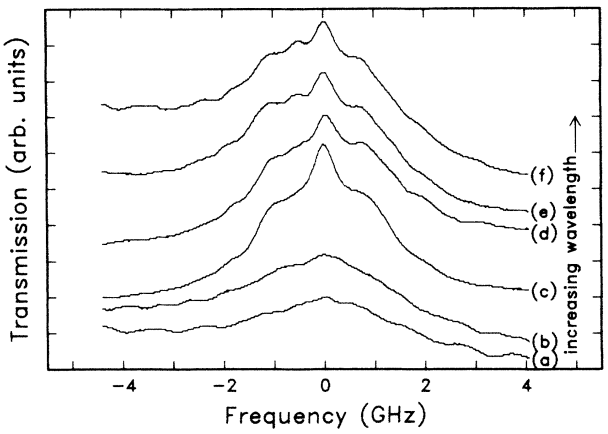

FIG. 3. Transmission spectra of holes burned at varying locations within the inhomogeneous ZPL absorption of R' centers in LiF + 0.2 mol% MgF_2. The burning intensity was 21 mW/cm^2, and the burning time was 1 s. The burn wavelengths were (a) 8325.29 Å, (b) 8325.48 Å, (c) 8329.98 Å, (d) 8335.18 Å, (e) 8335.39 Å, and (f) 8335.61 Å. The ZPL line center for this host was 8331.2 Å. All six traces have the same vertical scale, but the various traces have been offset for clarity.

of the ZPL, holes like traces (d)—(f) were typically observed. The most striking feature of the hole line shapes in Fig. 3 [especially visible in traces (c)—(f)] is the appearance of satellite or "side" holes, i.e., additional increases in transmission on both sides of the central peak.

Unfortunately, the side holes and the central hole overlap sufficiently such that detailed measurement of side-hole positions and widths cannot be easily performed.[25] Nevertheless, certain qualitative observations can be made. The hole shape shows no particular polarization anisotropy: holes burned with the polarization vector along either [100] or [110] show no change when scanned in the corresponding orthogonal polarization. Depending upon location in the ZPL, up to three side holes can be observed on the low-frequency side of the line and up to two side holes appear on the high-frequency side. Near the center of the ZPL [Fig. 3, trace (c)], two side holes typically appear on each side of the central peak, and the first set of side holes are spaced approximately ±1 GHz from the central hole while the very weak second set are approximately ±2 GHz away. This line shape is the one most commonly observed near the center of the ZPL. On the short-wavelength side of the ZPL [traces (a) and (b)], the side-hole structure is quite difficult to see and even the central peak is nonexistent, but on the long-wavelength side [traces (d), (e), and (f)], the high-frequency side holes appear to move closer to the central hole and a third low-frequency side hole appears at −500 MHz. The side holes appear to have widths roughly 50% larger than that of the central peak. Furthermore, the side holes are in most cases asymmetrical in depth and position with respect to the central hole. However, since the side-hole structure cannot be clearly resolved into distinct peaks, it is not easy to tell if a hole shape like trace (c) is composed of five broad holes alone or of five holes on top of a broad featureless hole similar to traces (a) and (b). The most that can be said from these data is that the strength and degree of asymmetry of the side holes clearly varies dramatically with position in the inhomogeneous line with an almost symmetrical line shape typically occurring near the center of the ZPL.

These observations about the dependence of the hole shape upon position in the ZPL together with similar observations for other host crystals (see Sec. III A 3 below) suggest that strain plays a role in the strength and position of the side holes. Part of the rest of this paper will be devoted to describing the effects of various perturbations on the side-hole structure, in order to attempt to infer their origin. It is worthwhile to note that any study of the effect of perturbations on side holes must keep careful track of position within the inhomogeneous line.

2. *Possible origins for the side holes*

In general, side holes reflect the presence of splittings in the excited state of the transition under study, just as antiholes can appear at the sums and differences of ground- and excited-state splittings when ground-state optical pumping occurs (as in nuclear-quadrupole optical hole burning[26]). In addition, side holes have been reported for PHB in certain defect centers in diamond.[27] Since no antiholes are observed in the present case, we can make no conclusions regarding the possibility of ground-state splittings. If the excited state is split into several sublevels and no selection rule prevents transitions from the ground state to the various excited-state sublevels, then side holes will appear at the value of and sums of the various excited-state splittings.

The R' center (a trigonal center with C_{3v} point group) has an origin transition of $^3A_2 \rightarrow {}^3E$ symmetry.[12,14] In zero magnetic field, the ^3E excited state can in the most general case split into three sublevels under uniaxial stress. Supposing that the three sublevels were split with splittings A and B, the expected hole spectrum can be deduced as follows: At different locations within the irradiated volume, the single-frequency burning laser would be resonant with each of the three excited-state sublevels, and the photochemical reaction would remove three groups of resonant centers from the absorption line. Now when the hole is probed, enhanced transmission would occur at each of the three transition energies possible for the first group, and similarly for the other two groups. The net effect for the general case is a central peak and three side holes symmetrically placed on each side of the central peak at spacings $\pm A$, $\pm B$, and $\pm(A+B)$.

Considering spectra like Fig. 3(c) which consists of five holes (central plus two roughly equally spaced side holes on each side), one would therefore conclude that the excited state splits into three equally spaced sublevels (i.e., $A=B$) with approximately 1 GHz spacing. Moreover, the asymmetric hole spectrum suggests that the hole-burning efficiency from the various excited-state sublevels is not constant. For the more complex hole spectra of traces (d)—(f), a different set of splittings would be implied. On the other hand, traces (a) and (b) seem to imply that on the short-wavelength side of the ZPL there is a wide dis-

tribution of splittings such that the side-hole structure is almost completely washed out.

Since the side-hole structure varies dramatically across the inhomogeneous line, we are tempted to associate the varying splittings with varying local uniaxial stresses. (For a discussion of external stress effects on the entire ZPL measured with linear-absorption spectroscopy, see Refs. 8 and 12.) In the presence of stress fields of varying symmetry and direction, the degeneracy of the ^3E excited state would be lifted to varying extents. It appears that as one moves across the ZPL, a changing distribution of local-uniaxial-stress values and directions gives rise to the varying hole shapes. The real puzzle that these data present is: why are the stress fields well-defined enough to give a clear set of side holes at certain locations within the ZPL? In the presence of *random* stress values, the side-hole structure would wash out and that may be the situation for traces (a) and (b). The only conclusion one can make in the regions of the ZPL in which the side holes are clearly visible is that the interaction that produces the inhomogeneous broadening is correlated with a well-defined local uniaxial stress. Furthermore, the asymmetry in the line shapes and the ratios of side-hole intensities indicates that the hole-burning efficiency is not constant among the various sublevels. We are led to the possibility that the R' centers are in some way associated with different types of nearby defects such as other color centers or perhaps ions introduced by the doping. Whether or not these defects are intrinsic is an important question, to be considered in the next section.

3. Dependence upon host crystal

To determine whether the Mg^{2+} ions or other dopant ions were responsible for the side holes, PHB experiments were performed in all host matrices listed in Table I. Of particular importance is the fact that side holes were clearly observed for the pure hosts as well as those doped with divalent or TLD dopants. Furthermore, the side holes in these other hosts also varied with position within the inhomogeneous line in a similar fashion. In fact, no dramatic systematic differences in hole shapes or dynamics were observed for R' centers in the various hosts that were larger than the changes in hole shape that occur for a single host as described above. In particular, changes in the host masses and spring constants produced by the isotopically enriched ^{6}LiF (TLD) samples did not observably affect the hole formation or dynamics. One may conclude that the PHB properties under observation here are not due to the various divalent dopant ions nor to phonon dynamics that depend upon the isotopic composition of the host crystal. This suggests that the side-hole structure is for the most part intrinsic to R' centers in x-irradiated (and γ-irradiated) LiF.

We note that in order to produce reasonable quantities of R' aggregate centers by x irradiation, far larger quantities of other color centers such as F or M centers are produced throughout the crystals. It seems plausible that local strain or electric fields from these "intrinsic" defects or other localized defects may be responsible for the unusual side-hole properties. For example, each R' center may be interacting with a distribution of other nearby color centers which produces a stress field that splits the ^3E excited state. Different locations within the inhomogeneous line appear to be influenced by different distributions of nearby perturbing centers. This illustrates the unique ability of PHB in uncovering local zero-field perturbations that are normally hidden in a broad, featureless inhomogeneously broadened line.

All other experiments reported in this paper were carried out using crystals of LiF:Mg^{2+} due to the ease of forming deep ZPL's in this system. As no strong systematic differences were observed for PHB among the various hosts listed in Table I, we feel that the results quoted here are generally applicable to the R' center in all the hosts listed.

4. Low-intensity limiting hole width

To understand relaxation processes for the R' center, it is important to determine the low-intensity limiting hole width for the central peak for cases where the central peak can be distinguished from the side holes. We assume that the central peak reflects the hole width of interest in the absence of splitting of the excited state. Accordingly, holes were burned for fixed burning time with lower and lower intensity until the limit of sensitivity was reached. Figure 4 shows examples of holes burned for 1 s each over two decades in burning intensity. The higher-intensity burns of traces (a) and (b) clearly show somewhat broader holes than the low-intensity burn of trace (c). For calibration, the relative hole depth of the central peak above the baseline for trace (c) was $\Delta T/T_i = 0.069$, where ΔT is the transmission change at the center of the hole and T_i is the initial transmission (before burning). By fitting three spectra like trace (c) to a phenomenological sum of Lorentzian line shapes for the central hole and two pairs of side holes, the low-intensity limiting width of the cen-

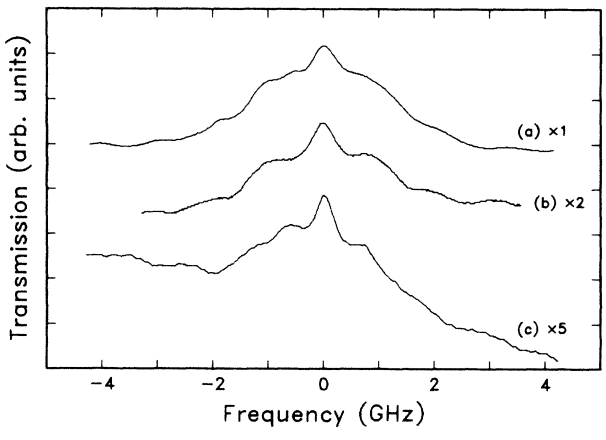

FIG. 4. Intensity dependence of spectral holes for R' centers in LiF + 0.2 mol% MgF_2. The burning time was 1 s, and the three traces have been offset and magnified where necessary for clarity. The burning intensities and wavelengths were (a) 22 mW/cm^2, 8334.02 Å; (b) 2.3 mW/cm^2, 8328.64 Å; and (c) 210 μW/cm^2, 8331.56 Å.

tral peak was estimated to be 600±50 MHz, FWHM.

This hole width is much larger than the 40—80 MHz widths observed for several aggregate color centers in NaF at shorter wavelengths.[2] Large hole widths have also been observed for another infrared color center in NaF.[11] The larger hole width cannot be due to power broadening because the saturation intensity for the R' system may be estimated[28] to be near 9 W/cm^2, whereas the largest intensity in Fig. 4 is 22 mW/cm^2. The hole width is certainly not lifetime-limited, because we have observed reasonably strong fluorescence from the R' center and have no reason to suspect that the excited-state lifetime is much shorter than the 10-ns value reported elsewhere.[29] It is possible that additional unknown dephasing effects are operating to broaden the holes beyond the lifetime-limited value, or that unknown spectral diffusion effects are responsible for the observed widths.

5. *Absence of hole-interaction effects*

Several previous studies of PHB for R' centers in LiF have mentioned a hole-interaction effect termed "self-erasing," in which the apparent size of a hole decreases after a second hole is burned nearby in frequency space.[16] In two recent reports the dependence of this effect on the distance between the holes in frequency space was measured.[18] All these previous measurements used derivative hole-detection techniques such as FM spectroscopy or wavelength modulation. Here we study the "self-erasing" effect using transmission detection of the spectral features so that the entire hole shape can be viewed easily.

Figure 5 shows a sequence of spectra of a portion of the inhomogeneous line as several holes are burned closer and closer together. In trace (a), a hole was burned at 8330.42 Å corresponding to 0 GHz in the figure. For trace (b), a second hole was burned + 5 GHz from the first. In trace (c) another hole was burned at −3 GHz, and in trace (d) a final hole was burned at −4.56 GHz. All four traces have been offset by an equal amount for comparison purposes. The results show that negligible degradation of already burned holes occurs when additional holes are burned as close as 1.56 GHz away. It appears that each new hole simply uses the line shape of the old hole as a background upon which the new hole is burned. We note in particular trace (d), in which the high-frequency side hole from the new burn gives a region of zero derivative that may look like a hole that is in between the new hole for trace (d) and the hole for trace (c).

We now seek to understand why previous studies observed a "self-erasing" effect with derivative detection while our transmission measurements appear to show negligible hole-interaction effects. Figure 6, trace (a) shows a hole measured in transmission similar to those in Fig. 5. Trace (b) shows the measured transmission spectrum after a new hole has been added at −1.5 GHz with no offset between the two traces, and negligible degradation of the original central peak has occurred. Trace (c) shows a derivative spectrum calculated from the transmission spectrum of trace (a), and trace (d) shows a derivative spectrum calculated from trace (b). The derivative spectrum of trace (d) seems to show self-erasing, if the peak-to-peak amplitude is used as a measure of the actual hole depth. Now, for an *isolated* hole of reasonable shape, the peak-to-peak amplitude of the derivative spectrum is proportional to the hole depth. However, when two holes are close together as in trace (d), the peak-to-peak amplitude of the derivative spectrum is not proportional to hole depth, because the steepness of the side of the central peak has decreased. In addition, the new hole is burned using as a baseline part of the original hole; since many centers had already been burned out of the line in the tail of the original hole, the resulting hole spectrum is not a linear superposition of the two hole shapes. Thus, the observation of a decrease in the amplitude of the derivative signal from the first hole can be explained without a "self-

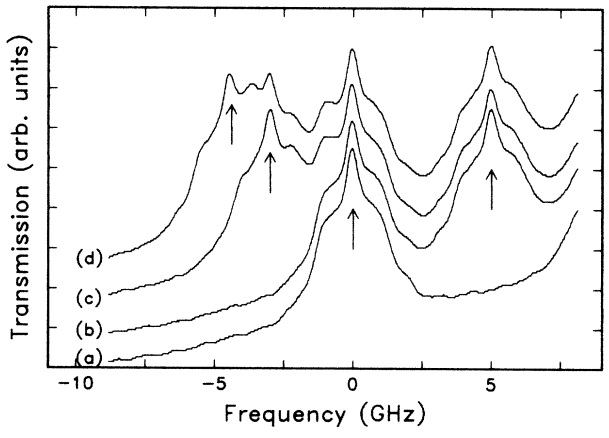

FIG. 5. Transmission spectra showing the absence of hole interaction effects for R' centers in LiF + 0.2 mol% MgF_2. Starting with trace (a), a new hole was added for each succeeding trace at the location of the arrow. All four traces have been offset by equal amounts for clarity. The burning time was 1 s and the burning intensity was 21 mW/cm^2 for each burn.

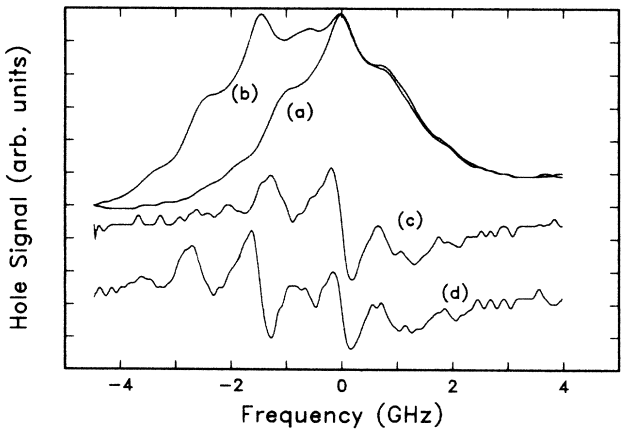

FIG. 6. Measured transmission spectra and calculated derivative spectra for R' centers in LiF + 0.05 mol% MgF_2 showing apparent "self-erasing" effects in the derivative traces. Legend: (a) A hole was burned for 1 s with an intensity of 27 mW/cm^2 at 0 GHz (8329.54 Å), (b) a second hole was burned at −1.5 GHz, (c) calculated derivative spectrum for trace (a), and (d) calculated derivative spectrum for trace (b).

erasing" effect. One would predict that whenever two holes are burned close enough together so that the tails of the holes overlap, degradation of the peak-to-peak derivative height would occur and the degradation would increase as the holes are burned closer and closer together. This observation has implications for derivative detection methods that might be used in actual readout of stored data. To prevent line-shape distortion and the appearance of spurious data, one would require that holes be placed no closer than approximately 4 GHz from one another in this material.

The lack of self-erasing effects for R' centers in LiF indicates that the hole-burning process forms a product state that does not absorb appreciably in the region of the hole itself. This is to be contrasted with some nonphotochemical mechanisms for hole burning[4] in which the product state does absorb in the spectral region of the hole. The lack of self-erasing effects for the R' center, coupled with the fact that uv radiation erases the holes slowly,[16,18] indicates that the process is indeed photochemical, probably resulting from electron tunneling away from the excited center and conversion of the R' center to a neutral R center. Unfortunately, experiments to detect increased absorption in the R band failed due to the fact that the area increase is spread over the entire R-center absorption.

B. Dynamics

1. Persistent hole lifetime and temperature cycling

Holes burned in the R'-center ZPL are quite stable at low temperatures: no observable degradation in hole depth at 1.4 K was observed for dark times on the order of 10 h. Furthermore, holes can withstand a certain amount of temperature cycling without complete annealing of the hole and reversal of the photochemical process. After allowing the cryostat to warm up to temperatures near 77 K overnight, holes from the previous day could regularly be observed, although with reduced amplitude and increased width. In particular, a spectral hole burned at 1.4 K withstood gradual warming to 20 K over a 2-h period and cooling back to 1.4 K over an additional 30-min period with negligible increase in hole width and only a 15% decrease in hole depth. Careful measurements of hole spectra as a function of annealing temperature in the future may allow a determination of irreversible spectral diffusion effects as well as the barrier height to reversal of the hole-burning process.

2. Transient holes detected with FM spectroscopy

Throughout this paper, the word "hole" without any qualifiers usually refers to persistent holes that last longer than any excited-state lifetime. An an unexpected result of FM spectroscopy measurements of the persistent holes, transient holes were also detected with a lifetime in the (10—100)-ms range. This section describes several examples of persistent and transient PHB using FM spectroscopy detection.

Figure 7 shows an example of PHB detection using the laser FM spectroscopy technique described in Sec. II C.

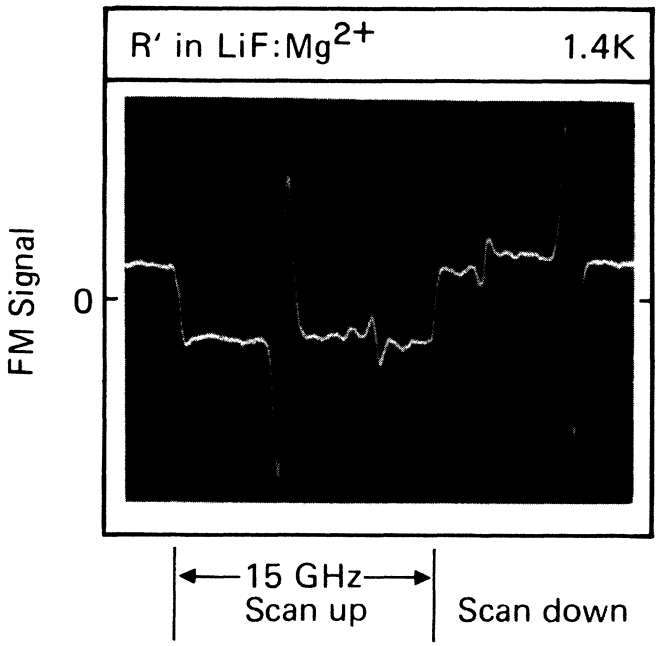

FIG. 7. FM signals resulting from PHB in LiF + 0.05 mol % MgF_2 at 1.4 K. The large signal results from reflection of the laser beam off a solid étalon before impinging on the detector. The laser frequency was held constant at the frequency corresponding to the center of the photograph for 30 s at a laser power of 10 mW to burn the hole shown. The scanning laser power was 10 μW in a 2-mm-diam spot, the burn wavelength was 8330.02 Å, and eight laser scans were averaged to produce the trace shown.

The vertical axis displays the (dc-coupled) mixer output as the laser frequency scans upward over a 15-GHz range in a sawtooth fashion every 0.25 s and then reverses. To calibrate the hole depth, the laser beam was reflected off a 10-GHz free-spectral-range solid étalon before impinging on the detector. Considering the upward laser scan first, the large derivative signal near the center of the scan results from the 50% deep absorption of the solid étalon. (Recall that as the widths of the spectral features become larger than the sideband spacing of 246 MHz, the FM signals approach the derivatives of the true absorption profiles.) The signal from a spectral hole burned for 30 s with a laser power of 10 mW in a 2-mm-diam spot appears at the exact center of the photograph. The hole shows the same side-hole structure discussed above. When the laser scan reverses (scan down), these spectral features appear again with the opposite polarity.

Figure 8 shows a spectral hole similar to that in Fig. 7 on an expanded frequency and amplitude scale. Viewing this trace as a derivative, the actual hole spectrum appears to have two shoulders or side holes on the low-frequency side located approximately 1 and 2 GHz from the center of the hole, and one strong shoulder on the high-frequency side 1 GHz from the center of the hole with perhaps a weak shoulder at 2 GHz. This side-hole structure compares well with the transmission spectra dis-

cussed above and clearly shows the utility of derivative spectra in enhancing the side-hole structure. However, derivative spectra are not sensitive to broad features in the wings of the holes.

The dc offsets that appear with opposite polarity in the upward and downward scans in Fig. 7 are an indication that transient holes are formed in addition to the persistent hole. Here a positive (or negative) FM signal means that the equality of the two sideband amplitudes has been unbalanced by the sample absorption, and the sign of the signal depends upon which sideband experiences more absorption and the setting of the phase shifter. We recall that as the laser scans, the trio of wavelengths representing the carrier and the two sidebands move together as a unit with a constant spacing. The fact that the sign of the FM signal depends upon the scan direction means that the leading sideband (in time) always sees more absorption than the trailing sideband. This strongly indicates that during reading the carrier is burning a transient hole which only the trailing sideband can experience. In order to observe such an effect, the transient hole must decay quickly on a timescale compared to the laser-scan period (0.25 s) but slowly on a scale compared to the time between the passage of the carrier and one sideband (4.1 ms).

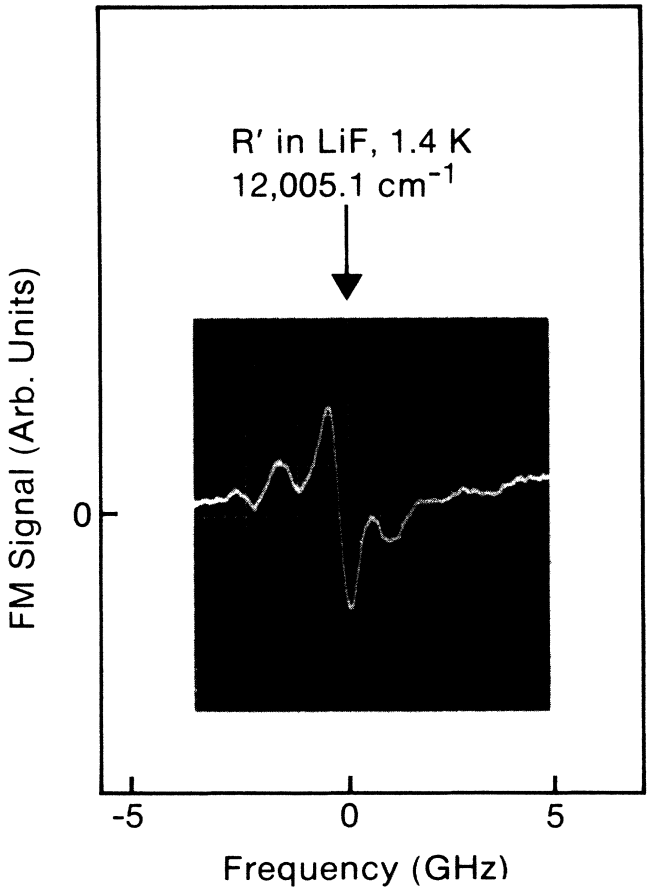

FIG. 8. FM spectrum of a single spectral hole burned in the R' center in LiF:Mg^{2+} ZPL origin absorption at 1.4 K. The burning and reading conditions are similar to Fig. 7, except that 64 scans were averaged to produce this trace.

Figure 9 shows a test of this hypothesis. The laser is repetitively scanned over a region of frequency space at which no persistent holes have been burned (with no averaging of the digitized mixer output). In part (a) of the figure the upward and downward scans each occur in 0.25 s, and the amplitudes of the resulting dc signals are equal. In part (b) the upward scan time has been increased to 2.5 s. Under these conditions the time between the passage of the carrier and a sideband has been increased by a factor of 10. As expected, the transient hole decays during this time period, so that the dc signal during upward scans is now quite small. During downward scans the dc signal is

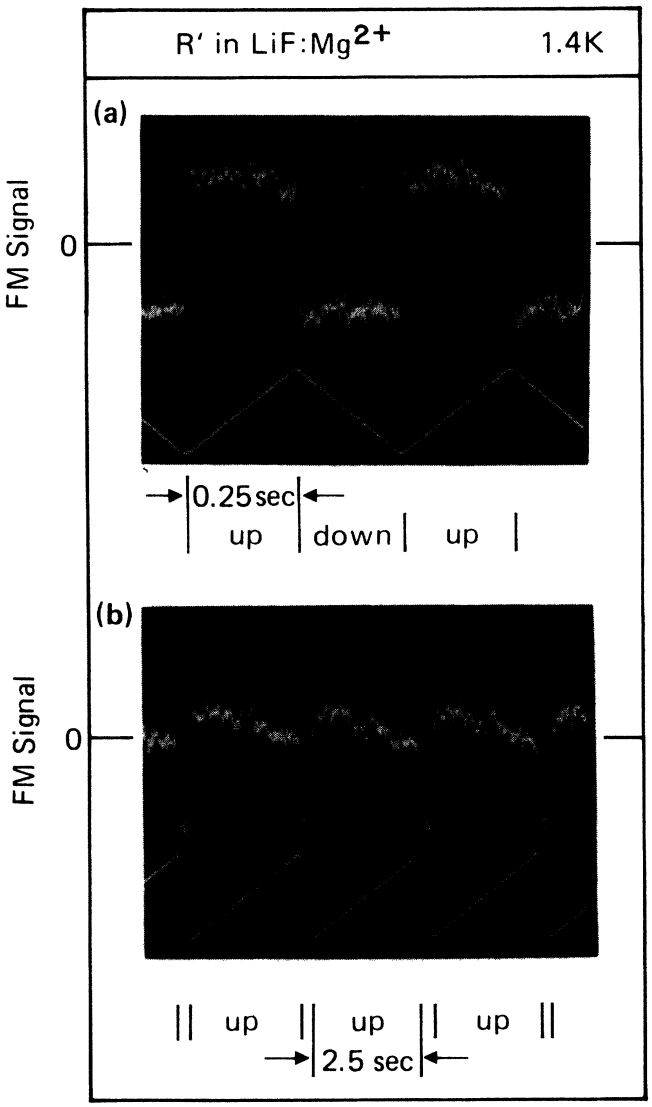

FIG. 9. Observation of transient hole-burning for R' centers in LiF:Mg^{2+} using laser FM spectroscopy. (a) The laser scan is symmetric, with 0.25 s for upward as well as downward scans. The laser scan covers a 15-GHz optical frequency range. The roles of positive and negative have been reversed compared to Fig. 7 using the phase shifter. The lower trace schematically depicts the instantaneous laser frequency. (b) Asymmetric laser scan: 2.5 s upward, 0.25 s downward. These traces were not averaged.

large as before.

We conclude that the bipolar dc offset is due to the burning of transient holes in the R'-center absorption, and that these transient holes have lifetimes in the range 4–40 ms. It is a useful feature of dc-coupled FM spectroscopy that such holes can easily be detected, suggesting the presence of long-lived intermediate states. Since the R' absorption is of $^3A_2 \rightarrow {}^3E$ character, the long-lived intermediate states are probably ^1E singlets or possibly quartets populated by intersystem crossing from the ^3E state. An important question is whether or not the hole-burning process proceeds through these intermediate states or through the ^3E state. One way to answer this question is to perform hole-burning measurements at constant burning energy, a method that has clearly shown the presence of bottlenecks in the burning cycle in other experiments.[30] We measured the hole depth for a burning energy of 6.2 μJ for burning times of 1 s, 100 ms, and 10 ms, and found $\Delta T/T_i = 0.069$, 0.055, and 0.029, respectively. This is evidence that the hole formation does proceed through an intermediate of lifetime in the (10–100)-ms range. Future experiments to observe the absorption spectrum and lifetime of these states by modulation spectroscopy and recovery of ground-state absorption should be attempted.

3. *Persistent hole growth: Typical data*

Figure 10 shows an example of the growth of the sample transmission measured at the center of the hole. Hole-growth dynamics can be quantified by measuring traces such as this for a variety of burning intensities. The y axis shows the laser power transmitted through the sample as a function of time as measured by the ratiometer described in Sec. II B. The laser beam was unblocked at $t = 0$ in a region of the ZPL in which no holes had previously been burned, and the time-varying transmitted signal (proportional to the sample transmission when the laser is unblocked) was recorded by a digital oscilloscope.

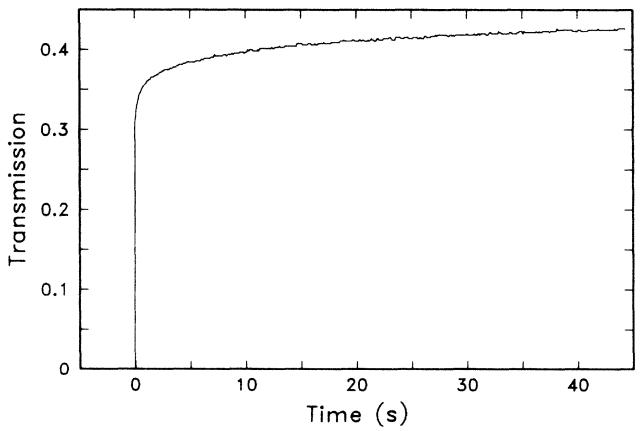

FIG. 10. Hole-growth curve for R' centers in LiF + 0.2 mol% MgF_2 at 1.4 K. The vertical axis shows the sample transmission derived from the laser power transmitted through the sample as a function of time since the unblocking of the laser beam at $t = 0$. The ratiometer time constant was 3 ms and the laser intensity was 21 mW/cm^2.

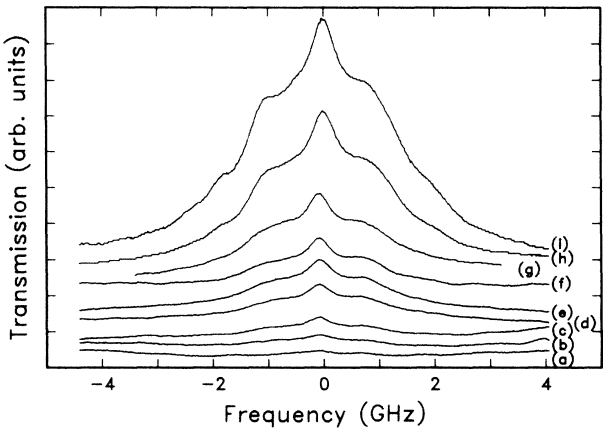

FIG. 11. Time dependence of hole shape at constant burning intensity of 20 mW/cm^2. All holes were burned near the center of the ZPL for R' centers in LiF + 0.2 mol% MgF_2. The burning times were (a) 1 ms, (b) 2 ms, (c) 5 ms, (d) 10 ms, (e) 20 ms, (f) 50 ms, (g) 100 ms, (h) 1 s, and (i) 10 s. All traces have the same gain, but individual traces have been offset for clarity.

The constant intensity probe beam serves to both burn and detect the spectral hole as it grows. We note that the total transmitted signal measures the increase in transmission due to the transient hole as well as the persistent hole. However, since the times of interest along the horizontal axis are much longer than the lifetime of the intermediate state, the transient hole contributes only a constant offset to the signal in Fig. 10.

To complement time-domain traces like Fig. 10, Fig. 11 shows transmission spectra of persistent holes acquired at constant burning intensity over a range of burning times using the methods described in Sec. II B. Starting at the bottom of the figure, the burning time increases from 1 ms [trace (a)] up to 10 s [trace (i)], with the actual burning times for all the other traces listed in the figure caption. For each trace the burning wavelength was shifted by 0.1–0.2 Å so that each hole would be burned in a virgin region of the inhomogeneous line. For calibration, trace (i) corresponds to a transmission change from 0.34 before burning to 0.48 at the center of the hole after burning, so $\Delta T/T_i = 0.41$ for this trace. It appears that the hole depth is saturating, but more careful study of the hole kinetics below shows that this is not the case. It is clear that for short burning times the side-hole structure is not so easily detected, but that for long burning times the side-hole structure is quite apparent. The detailed time dependence of the hole growth at 0 GHz will be presented in more detail below.

4. *Persistent hole growth: Effective quantum efficiency*

One benchmark parameter of the hole-growth dynamics is the effective hole-burning quantum efficiency at small burning time, η. This quantity can be estimated using the $t = 0$ time derivative of the sample transmission recorded during the growth of a spectral hole, as in Fig. 10. This technique, described more fully in Ref. 31, assumes that

the hole kinetics are first order, which is a reasonable approximation for almost any process near enough to $t=0$. The actual hole-growth dynamics for $t>0$, are, in fact, quite complex and clearly nonexponential, as will be described below. Nevertheless, the estimation of η provides a useful quantity for comparison with the value of η for other systems. We emphasize that the derivative is computed for times longer than the growth time of the transient holes described in the preceding subsection, so that the effect of the transient holes is only to reduce the excitation power somewhat.

Estimation of η requires knowledge of σ, the low-temperature peak absorption cross section for molecules within a homogeneous linewidth of the laser frequency.[31] The calculation of σ, in turn, requires knowledge of the oscillator strength for the ZPL, and the measured hole width at low temperatures. We use values of $f=0.02$ (a reasonable estimate for the oscillator strength attributable to the ZPL for R' centers) and $\Delta\nu_{\text{hole}}=625$ MHz measured from the hole spectra. This yields an estimate for the cross section $\sigma=1.3\times10^{-12}$ cm^2. Using the measured values $(dT/dt)|_{t=0}=0.10$ s^{-1}, $T_i=0.31$, and laser intensity 21 mW/cm^2, we estimate the hole-burning efficiency η to be 4×10^{-6}. This estimate is probably useful only to within an order of magnitude owing to the uncertainties in the oscillator strength and T_i.

The PHB efficiency for the R' system is similar to the 10^{-6} efficiencies characteristic of most other color centers[2] in alkali halides. It is clearly much smaller than the quite large (10^{-2}) value of η observed for the 8892-Å color center in electron-irradiated NaF.[11] The low value of η for R' centers in LiF suggests that the hole-formation process involves tunneling over high barriers or perhaps a two-photon stepwise process. Since the hole-growth rate is not quadratic in the burning power (see below), a two-photon process for hole formation is unlikely. In previous work[32,22] bleaching of the R' absorption occurred if samples were irradiated with R-band light near 4000 Å, suggesting that the excited state of the R' is about 1.5 eV below the conduction band. Future experiments should search for two-color photon-gated hole production[33,34] in this system.

5. *Persistent hole growth: Detailed dynamics at line center*

To further probe the dynamics of the persistent hole-formation process, hole-growth curves similar to Figs. 10 and 11 were analyzed in detail. The intent here is to explain the time dependence of hole growth using a phenomenological or even a microscopic model for the hole-burning process as has been done for other systems.[4,11] Figure 12 shows the relative hole depth $\Delta T/T_i$ versus time for burning powers varying over more than 3 orders of magnitude. For small values of $\Delta T/T_i$, the relative hole depth so defined is approximately equal to $(\Delta\alpha)L$, where $\Delta\alpha$ is the absorption-coefficient change at the hole center and L is the sample length. A logarithmic time plot was found to represent the data better than log-log or exponential plots.[35] For the highest burning power [trace (a)], the data follow a logarithmic time dependence quite well over more than 2.5 orders of magnitude in time

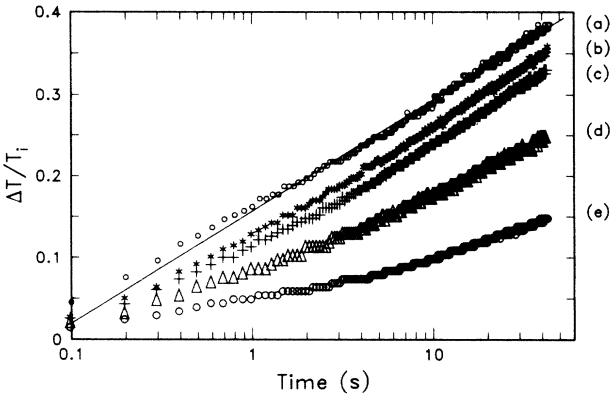

FIG. 12. Relative hole depth versus time for several burning intensities for R' centers in LiF + 0.2 mol% MgF_2. The burning intensities were (a) 21 mW/cm^2, (b) 6.0 mW/cm^2, (c) 570 μW/cm^2, (d) 60 μW/cm^2, and (e) 4.5 μW/cm^2. The straight line is a least-squares log-time fit to trace (a) with standard deviation 0.0041. The ratiometer time constant was 3 ms.

with a small departure from a log time dependence at times less than 1 s. Approximate logarithmic time behavior is observed for lower burning powers, with larger departures from this dependence at small burning time. (This departure must eventually occur, because the hole depth can only be rigorously zero at $t=0$). The straight line in the figure is a least-squares fit to the data of trace (a). It is clear that usual first-order kinetics cannot explain this logarithmic time dependence. To our knowledge, this is the first observation of such growth dynamics for spectral hole burning.

To confirm that this logarithmic time behavior is not an artifact of the measurement technique arising from the transient holes described in Sec. III B 2, persistent hole depths as a function of burning time were determined from actual spectra of the persistent hole similar to those in Fig. 11. The result is shown in Fig. 13 and again a logarithmic time plot represents the data better than either

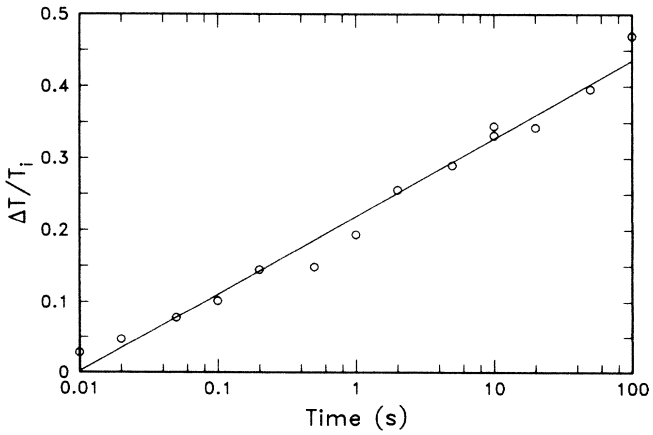

FIG. 13. Relative hole depth versus burning time for a series of hole spectra similar to Fig. 11. The burning intensity was 23 mW/cm^2. The straight line is a least-squares fit to the data with standard deviation 0.020.

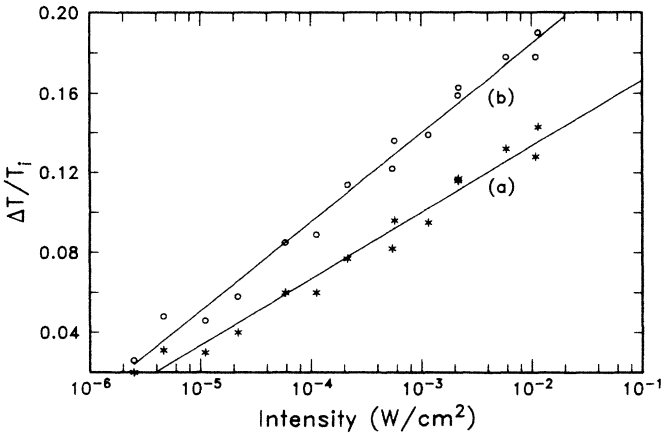

FIG. 14. Relative hole depth versus burning intensity for (a) $t=1$ s and (b) $t=2.5$ s for the sample of Fig. 11. The straight lines are least-squares fits to the data.

an algebraic or exponential form over 4 orders of magnitude in burning time. The straight line in Fig. 13 is a least-squares fit to the data.

In our preliminary report of PHB for the R' center in LiF,[16] a logarithmic dependence of hole depth upon burning fluence ($t_B I$) was presented, where t_B is the burning time and I is the burning intensity in W/cm^2. We emphasize that this result was obtained for burning intensities greater than or equal to 0.7 W/cm^2. At lower burning intensity, the hole-growth dynamics are more complex. To measure hole growth as a function of burning intensity, the relative hole depth after a fixed burning time was determined from a series of growth curves like Fig. 10. Figure 14 shows the result for two burning times: the relative hole depth is proportional to the logarithm of the intensity in both cases over more than 3 orders of magnitude. One might be tempted to conclude that the hole growth in the low-intensity regime also follows a log fluence form; however, attempts to fit the growth data of Figs. 12 and 14 to the fluence do not produce a universal curve. For example, Fig. 15 shows the result if the data of Fig. 12 are replotted as a function of fluence. It appears that the growth curves are approaching a log fluence dependence at the highest burning intensity [trace (a)]. Thus these results are in good agreement with the data presented in Ref. 16 which began at a fluence of 0.1 J/cm^2 and an intensity of 0.7 W/cm^2. Such novel fluence, intensity, and time dependences show that the kinetics of PHB for R' centers in LiF are particularly interesting.

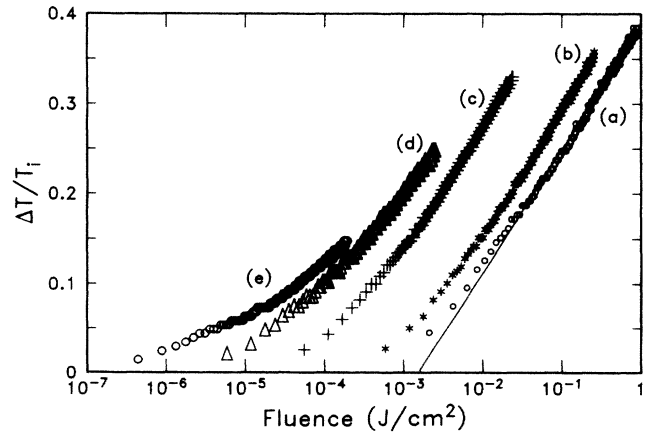

FIG. 15. Relative hole depth versus burning fluence for the sample of Fig. 12. The burning intensities were (a) 21 mW/cm^2, (b) 6.0 mW/cm^2, (c) 570 μW/cm^2, (d) 60 μW/cm^2, and (e) 4.5 μW/cm^2.

6. *Tunneling model for hole growth*

These unusual growth kinetics provide fertile ground for possible theoretical models for the microscopic mechanism for PHB in this color-center system. Previous models for the hole growth based on center reorientation[4] and on first-order kinetics with constant quantum efficiency[11] do not fit the data for the R' center. On the other hand, logarithmic time dependences have been observed in the time dependence of specific heat of amorphous solids, to give one example.[36] In fact, logarithmic *decay* of spectral holes in a system with proton tunneling[37] has been observed and modeled assuming a coupling to a broad distribution of two-level systems (TLS's).[38] We are led to present the following phenomenological model for the hole growth in which the various R' centers are coupled to a distribution of tunneling states that represent the electron-trapping and hole-formation mechanism.

Figure 16 schematically shows the process. Light of flux F (photons/s cm^2) excites transitions from $^3A_2$ to ^3E with excitation rate σF. Any splitting of ^3E is ignored for the purposes of explaining the growth data at line center. From the triplet excited state, the system returns to the ground state with rate Γ_1 via radiative and nonradiative channels or intersystem crosses with rate Γ_{1m} to an intermediate state or states, m. The transient hole studies of Sec. III B 2 above suggest that state m has a lifetime in the range 4—40 ms; hence, the decay rate $\Gamma_m = (4\text{—}40\ \text{ms})^{-1}$. State m is to be viewed as the "left well" of a distribution of asymmetric two-level systems that represent the tunneling process. In this model, we ignore reverse

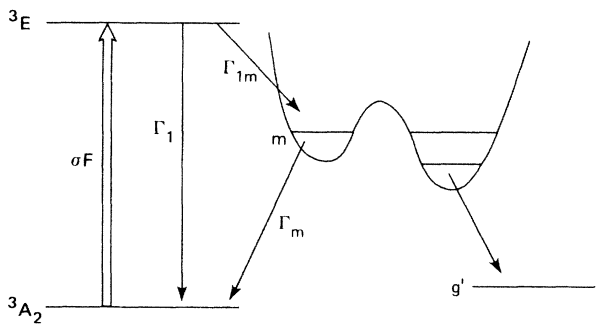

FIG. 16. Schematic of the suggested mechanism for hole formation. The cross section for the $^3A_2 \rightarrow {}^3E$ transition is σ, the pumping flux is F, Γ_1 is the decay rate to the ground state from ^3E, Γ_{1m} is the rate populating intermediate state m, Γ_m is the decay rate from state m back to the $^3A_2$ ground state, and g' is the product ground state.

tunneling for simplicity, i.e., we assume that if electron tunneling occurs to the "right well" via a phonon-assisted process, for example, then the electron eventually enters a new ground state g' representing the electron trap and the center no longer absorbs at the laser wavelength.

Following the arguments of Anderson *et al.*,[38] we assume that the ensemble of TLS's in the sample contains a broad (uniformly distributed[39]) range of asymmetries and tunneling splittings, which reflects our physical assumption that the various centers have different nearby traps for the ejected electron. Jäckle[40] has shown that for this type of TLS distribution, the distribution $P(R)$ of tunneling rates R varies as

$$P(R)=(R_0/2)\frac{1}{R(1-R/R_{\max})^{1/2}}\ , \tag{1}$$

where R_0 is a constant and $R_{\max}$ is the rate for zero asymmetry and total energy equal to the tunneling splitting. Now to produce a simple model, we note that although several traps may be associated with each center in the sample, only the trap with the largest tunneling rate is important for any given center. Thus each center in the sample may in an approximate way be indexed by the tunneling rate R of its primary TLS, and therefore $P(R)$ may be used as the distribution for R' centers. In this case, the number of centers that react (tunnel) after a given time just depends on the distribution of rates that are available.

To derive an expression for the time dependence of the number of centers we use a modification of the approach of Ref. 37. The normalization of Eq. (1) may be achieved by assuming that there exists for any system a minimum tunneling rate $R_{\min}$ that reflects an upper limit on the barrier heights. There is also a maximum tunneling rate $R_{\max}$ that occurs for centers coupled to TLS's that have zero asymmetry and low barrier heights. We asume that if the centers are irradiated for a sufficiently long time, then all centers (in resonance) will eventually react. Thus, integration of Eq. (1) from $R_{\min}$ to $R_{\max}$ should just produce the total number of centers within a homogeneous width of the laser frequency, N_0.

To derive an approximation to the number of centers that have reacted after time t at burning intensity I, $N(t,I)$, one need only integrate Eq. (1) from the smallest rate that can contribute to the largest rate that can contribute. The smallest rate that can contribute in time t is bounded by the reciprocal of the observation time, $1/t$. In the regime where the overall reaction rate is limited by the light excitation and not by the tunneling systems, the maximum rate is bounded by the excitation rate $\sigma I/h\nu$, where h is Planck's constant and ν is the frequency of the laser beam. Thus we have that

$$\frac{N(t,I)}{N_0}=[\ln(4R_{\max}/R_{\min})]^{-1}\times\int_{1/t}^{\sigma I/h\nu}dR\frac{1}{R(1-R/R_{\max})^{1/2}}\ . \tag{2}$$

The result of the integration is logarithmic growth of the hole of the form

$$\frac{\Delta T}{T_i}(t,I)=(\alpha_i L)\frac{N(t,I)}{N_0}=(\alpha_i L)\frac{\ln(\sigma I t/h\nu)}{\ln(4R_{\max}/R_{\min})}\ , \tag{3}$$

where α_i is the initial absorption coefficient, L is the sample length, $\Delta T/T_i$ has been assumed small compared to 1, and where $R_{\min}\ll 1/t\ll\sigma I/h\nu\ll R_{\max}$. For simplicity, we have ignored the dynamics of the hole width, assuming that the value of the absorption coefficient at the center of the hole is proportional to the hole area. Thus, this simple phenomenological tunneling model predicts a logarithmic growth of the spectral hole at line center as a function of the burning fluence (assuming constant hole width).

Over the past decade, the TLS model[38] has been most successful in explaining ground-state tunneling processes in amorphous systems.[36] It has also been applied to ground-state PHB decay experiments.[37] We realize from the outset that the simple extension presented here cannot be a complete description of the excited-state tunneling process occurring for R' centers in LiF. In particular, many of the unusual properties of amorphous systems are driven by the extremely slow relaxations that can occur on long timescales, but these long timescales probably do not affect the R'-center growth because the intermediate-state lifetime is only on the order of 10 ms. We thus welcome future theoretical efforts toward a more complete description.

In spite of the sweeping assumptions leading to Eq. (3), this simple model correctly describes the log fluence dependence in the high-intensity regime presented in Ref. 16 and in Fig. 15, trace (a). The least-squares fit to the latter is of the form $a+b\ln(tI)$, with $a=0.387$ and $b=0.0595$. From these fitting parameters and the fact that $T_i=0.31$, one can deduce from the slope of the logarithmic fit that $R_{\max}/R_{\min}=9.8\times10^7$. To the level of approximation in use here, this ratio may be viewed as an approximate measure of the width of the TLS distribution, and the distribution does cover a fairly broad range of tunneling rates.

The measured time and fluence dependence of the data at lower intensities depart from the simple model of Eq. (3) for any of a variety of possible reasons: breakdown of the assumption that the photon excitation rate is a reasonable estimate of the maximum tunneling rate, breakdown of the assumption of a uniform distribution of tunneling systems, unknown details of the actual level structure and relaxation rates for the optical transitions, etc. On the other hand, the intensity dependence alone in Fig. 14 follows Eq. (3) quite well, but the physical reasons for this effect are unclear. Nevertheless, the success of this phenomenological tunneling model for the PHB dynamics leads one to speculate on the nature of the traps with which the various centers interact. It appears that the R' aggregates are to a first approximation embedded in a sea of traps with widely varying distances from the centers and barrier heights to tunneling. Coupling this result with the static hole-shape measurements of Sec. III A, we are again led to postulate that the bath of color centers other than R' centers in the sample are the source of both varying uniaxial stresses and deep trapping sites for electrons. In a sense, then, the data suggest that R' centers in

x-irradiated single crystals of LiF interact with a random distribution of TLS's that show dynamics similar to that for amorphous glasses and polymers. This analysis of hole-growth kinetics illustrates the power of PHB in uncovering novel details of local dynamics of impurity centers in solids. To look for a clearer signature of the phonon-induced tunneling process, future experiments should consider measuring the temperature dependence of the R' hole-growth dynamics.

C. Effect of external fields

1. Stark effect

To learn more about the effect of various external perturbations on spectral holes in the R'-center ZPL absorption, a series of Stark-effect measurements were completed. The electric field vector of the infrared laser beam was chosen parallel to the dc electric field vector, which was aligned along a [100] axis. In all cases, the light-propagation vector was parallel to [001]. Figure 17 shows the hole spectra for a variety of dc fields. Here a hole was burned in zero field [trace (a), bottom], and then the field was increased monotonically [traces (b)—(m)] and then returned to zero [trace (n), top].

The Stark effect of spectral holes in color centers has been used to advantage in the determination of exact symmetries of several ZPL's in NaF.[2,41] For the R' center in LiF, the width of the central hole and the interference from the side holes makes clear observation of a Stark splitting somewhat difficult. In fact, the most obvious effect of the external field is simply to appear to wash out the hole structure, a phenomenon that may have some practical applications which will be mentioned below. Nevertheless, a hint of a splitting of the central feature is evident in the figure in traces (g)—(k). Plotting the splitting as a function of field yields a linear Stark effect with field sensitivity of 0.14 MHz/V cm^{-1} for each component. We observed similar results for pure (natural) LiF as well. This result compares favorably with the linear Stark effect observed by Davis and Fitchen,[42] who measured the value of 0.12 MHz/V cm^{-1} for the same geometry by applying 100-times-larger fields and measuring the splitting of the entire R' ZPL with linear spectroscopy.

Stark spectra were also measured for the infrared polarization perpendicular to the dc electric field, which remained parallel to the [100] axis. Figure 18 shows the results with zero field at the bottom [trace (a)], increasing field up to trace (j), and zero field again for trace (k). For this orientation the line splits into more components, and the broad pedestal from the side holes precludes any estimate of Stark-splitting coefficients. The overall effect is a smearing of the transmission increase due to the hole over a wider and wider range of the ZPL until the hole is essentially no longer visible.

Figure 19 shows how this effect may be used to some advantage to provide an additional dimension for the burning of spectral holes. In trace (a), a hole was burned at 0 GHz, 0 kV, and scanned at 0 kV. In trace (b), a new hole was burned at 0 GHz, 2 kV, and scanned at 2 kV. In trace (c), the same spectral region was scanned at 1 kV; only weak traces of both previously burned holes can be observed. In trace (d), a new hole was burned at $+3.9$ GHz, 2 kV, and scanned at 2 kV. Finally, in trace (e), the line was scanned again at 0 kV; the hole at $+3.9$ GHz is essentially unobservable. These results show that to a limited extent a new spectrum of holes can be burned at each of several widely spaced field values, a property that may be of use in frequency-domain optical-storage applica-

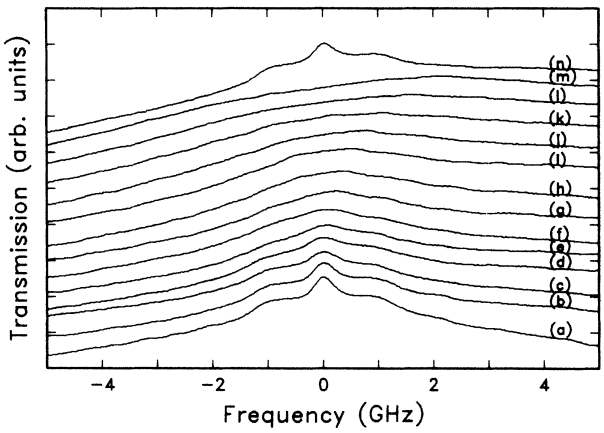

FIG. 17. Stark effect for spectral holes in the R' ZPL in LiF + 0.2 mol% MgF_2 at 1.4 K for optical field parallel to dc field parallel to [100]. The hole in (a) was burned in zero field for 100 s at a laser intensity of 200 μW/cm^2. The fields for the other traces were (b) 371 V/cm, (c) 743 V/cm, (d) 1.11×10^3 V/cm (e) 1.49×10^3 V/cm, (f) 1.86×10^3 V/cm, (g) 2.23×10^3 V/cm, (h) 2.98×10^3 V/cm, (i) 3.72×10^3 V/cm, (j) 5.58×10^3 V/cm, (k) 7.43×10^3 V/cm, (l) 1.12×10^4 V/cm, (m) 1.49×10^4 V/cm, and (n) 0 V/cm. The traces have been offset vertically for clarity.

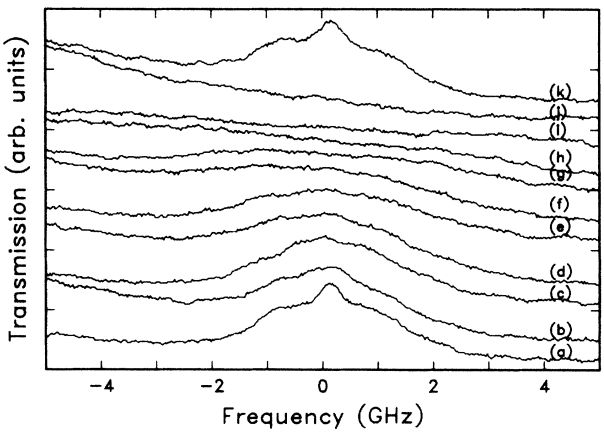

FIG. 18. Stark effect of spectral holes for the case of optical field perpendicular to dc field, which was parallel to [100]. The hole in (a) was burned in zero field for 100 s with a laser intensity of 190 μW/cm^2. The fields for the other traces were (b) 413 V/cm, (c) 826 V/cm, (d) 1.24×10^3 V/cm, (e) 1.65×10^3 V/cm, (f) 2.07×10^3 V/cm, (g) 2.48×10^3 V/cm, (h) 3.31×10^3 V/cm, (i) 4.13×10^3 V/cm, (j) 8.26×10^3 V/cm, and (k) 0 V/cm. The traces have been offset vertically for clarity.

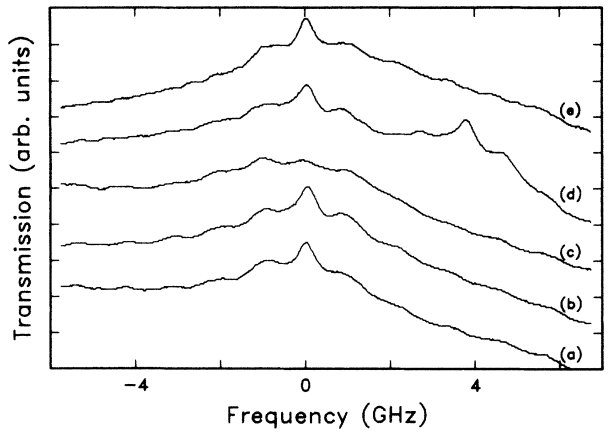

FIG. 19. Transmission spectra of holes burned with and without applied fields for the orientation of Fig. 17. Legend: (a) hole burned at 0 kV, scanned with 0 kV; (b) new hole burned at 0 GHz at 2 kV, scanned at 2 kV; (c) scan at 1 kV; (d) new hole added at 3.9 GHz at 2 kV, scanned at 2 kV; (e) scan at 0 kV. The sample thickness was 0.134 cm. The traces have been offset vertically for clarity.

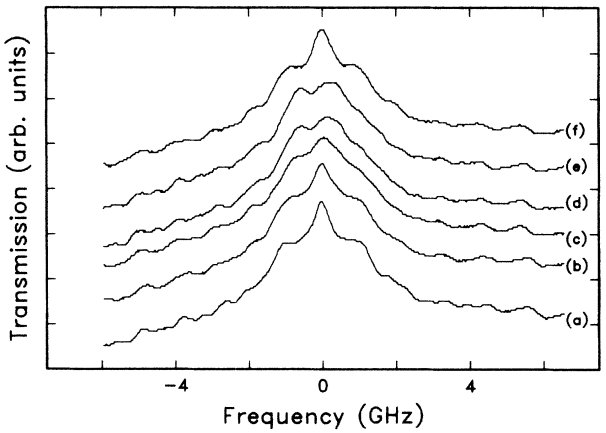

FIG. 20. Zeeman effect for spectral holes in the R'-center absorption. The magnetic and optical electric fields were both parallel to [100]. The applied magnetic fields were (a) 0 G, (b) 80 G, (c) 160 G, (d) 240 G, (e) 320 G, and (f) 0 G. The traces have been offset vertically for clarity.

tions. This fact has been mentioned previously by several authors.[43–46] Here inhomogeneous electric fields were not required: the effect depends upon the property of the spectral holes to essentially disappear into the background of the inhomogeneous line for sufficiently different applied fields.

2. *Zeeman effect*

As a final example of the effect of external fields on spectral holes for R' centers in LiF, magnetic fields were applied to the sample using a pair of small Helmholtz coils. Here only qualitative studies could be performed for reasons to be described below. The optical electric field and the magnetic field were both aligned along a [100] direction, and the light-propagation vector was parallel to [001]. For this configuration, a trigonal $A \rightarrow E$ transition should split into two components. Figure 20 shows the effect of magnetic field on a hole burned for 100 s with a laser intensity of 230 μW/cm^2. The field increases from 0 G in trace (a) up to 320 G for trace (e) (the maximum field for our coils) and then returns to 0 G for trace (f).

It is clear that obtaining a definitive set of Zeeman splittings from data like Fig. 20 is complicated by the weak Fabry-Perot structure in the baseline, the maximum field available, and the width of the central peak and the side holes. One may qualitatively observe that the central peak appears to broaden and shift slightly to higher frequency suggestive of a splitting. This is additional evidence that the central peak is partly due to centers with zero stress splitting. The low-frequency side hole grows slightly and moves up in frequency while the high-frequency side hole almost disappears. The source of these effects is unknown at present, and in addition, the side holes show different properties at different locations in the inhomogeneous line. The strong reduction in the orbital moment due to a dynamic Jahn-Teller effect[13,14] partially accounts for the small size of the observed splittings. Magnetic circular dichroism measurements of the spectral holes in the future should provide more complete information.

IV. CONCLUSION

We have reported the statics, dynamics, and effect of external magnetic and electric fields on spectral holes for the R'-center ZPL absorption in LiF. The hole shape contains a central peak with a side-hole structure that varies as a function of position in the inhomogeneous line most strongly in the wings, suggesting a quasi-random splitting of the excited state due to fairly well-defined local stresses in the crystal. The source of the changes in the side-hole structure may be the presence of other nearby F-, M-, and R-center defects produced by the coloring process. Furthermore, the fact that fairly well-defined hole shapes appear in some parts of the ZPL absorption suggests that the local environments of some of the R' centers are similar. The hole-growth kinetics are nonexponential, showing a logarithmic time and intensity dependence over several decades, and a logarithmic fluence dependence at higher intensities. A simple tunneling model that assumes that the bath of R' centers is coupled to a random distribution of barriers to tunneling gives a preliminary microscopic foundation for the logarithmic fluence dependence. The Stark and Zeeman effects are consistent with previous data and the postulated splitting of the ^3E excited state. These results illustrate the power of PHB measurements in uncovering dynamics and statics hidden within inhomogeneously broadened lines. In particular, other photoionization processes for PHB in which the trap states are randomly distributed throughout the host may be expected to show logarithmic time dependences.[33,34] It is hoped that with the publication of these results, theoretical interest will be stimulated in the interesting properties of this and other systems showing PHB.

ACKNOWLEDGMENTS

The authors acknowledge useful and stimulating discussions with R. Harley, C. Ortiz, and H. Morawitz on some of the results reported in this paper. The authors thank R. Marbury of Harshaw Chemical Company for supplying a crystal of ^{7}LiF and R. M. Macfarlane for the loan of a Stark-effect sample holder and a pair of Helmholtz coils. This work was supported in part by the U.S. Office of Naval Research.

---

*Present address: IBM Sindelfingen, Sindelfingen, West Germany.

[1]L. A. Rebane, A. A. Gorokhovskii, and J. V. Kikas, Appl. Phys. B **29**, 235 (1982).

[2]R. M. Macfarlane, R. T. Harley, and R. M. Shelby, Radiat. Eff. **72**, 1 (1983); R. M. Macfarlane and R. M. Shelby, Cryst. Lattice Defects Amorph. Mater. **12**, 417 (1985).

[3]J. Friedrich and D. Haarer, Angew. Chem. Int. Eng. Ed. **23**, 113 (1984).

[4]W. E. Moerner, A. J. Sievers, R. H. Silsbee, A. R. Chraplyvy, and D. K. Lambert, Phys. Rev. Lett. **49**, 398 (1982); W. E. Moerner, A. R. Chraplyvy, A. J. Sievers, and R. H. Silsbee, Phys. Rev. B **28**, 7244 (1983).

[5]G. J. Small, in *Spectroscopy and Excitation Dynamics of Condensed Molecular Systems,* edited by V. M. Agranovitch and R. M. Hochstrasser (North-Holland, Amsterdam, 1983), pp. 515–554.

[6]G. Castro, D. Haarer, R. M. Macfarlane, and H. P. Trommsdorff, U.S. Patent No. 4 101 976 (1978).

[7]W. E. Moerner, J. Mol. Elec. **1**, 55 (1985), and references therein.

[8]For a review, see D. B. Fitchen, in *Physics of Color Centers,* edited by W. B. Fowler (Academic, New York, 1968), pp. 293–350.

[9]R. M. Macfarlane and R. M. Shelby, Phys. Rev. Lett. **42**, 788 (1979).

[10]M. D. Levenson, R. M. Macfarlane, and R. M. Shelby, Phys. Rev. B **22**, 4915 (1980).

[11]W. E. Moerner, F. M. Schellenberg, G. C. Bjorklund, P. Kaipa, and F. Lüty, Phys. Rev. B **32**, 1270 (1985).

[12]D. B. Fitchen, H. R. Fetterman, and C. B. Pierce, Solid State Commun. **4**, 205 (1966).

[13]H. R. Fetterman and D. B. Fitchen, Solid State Commun. **6**, 501 (1968).

[14]J. A. Davis and D. B. Fitchen, Solid State Commun. **6**, 505 (1968).

[15]W. E. Moerner, F. M. Schellenberg, and G. C. Bjorklund, Appl. Phys. B **28**, 263 (1982); W. E. Moerner, P. Pokrowsky, and G. C. Bjorklund, Bull. Am. Phys. Soc. **28**, 451 (1983).

[16]P. Pokrowsky, W. E. Moerner, F. Chu, and G. C. Bjorklund, Opt. Lett. **8**, 280 (1983); P. Pokrowsky, W. E. Moerner, F. Chu, and G. C. Bjorklund, Proc. Soc. Photo-Opt. Instrum. Eng. **382**, 202 (1983).

[17]H. W. H. Lee, A. L. Huston, M. Gehrtz, and W. E. Moerner, Chem. Phys. Lett. **114**, 491 (1985).

[18]C. Ortiz, C. N. Afonso, P. Pokrowsky, and G. C. Bjorklund, Appl. Phys. Lett. **43**, 1102 (1983); C. Ortiz, C. N. Afonso, P. Pokrowsky, and G. C. Bjorklund, Nucl. Instrum. Methods Phys. Res. B **1**, 469 (1984).

[19]C. Ortiz, C. N. Afonso, M. Gehrtz, F. M. Schellenberg, G. C. Bjorklund, and E. A. Whittaker, Appl. Phys. B (to be published).

[20]G. C. Bjorklund, Opt. Lett. **5**, 15 (1980); G. C. Bjorklund, M. D. Levenson, W. Lenth, and C. Ortiz, Appl. Phys. B **32**, (1983).

[21]Cornell University Crystal Growing Facility, Materials Science Center, Cornell University, Ithaca, N.Y.

[22]A. E. Hughes, Solid State Commun. **4**, 337 (1966); A. E. Hughes, Ph.D. thesis, Oxford University, 1966.

[23]M. D. Levenson, W. E. Moerner, and D. E. Horne, Opt. Lett. **8**, 108 (1983).

[24]M. Gehrtz, E. A. Whittaker, and G. C. Bjorklund, J. Opt. Soc. Am. B **2**, 1510 (1985).

[25]Some deconvolutions of the hole line shape for specific hosts appear in Ref. 19.

[26]R. M. Macfarlane, R. M. Shelby, A. Z. Genack, and D. A. Weitz, Opt. Lett. **5**, 462 (1980).

[27]R. T. Harley, M. J. Henderson, and R. M. Macfarlane, J. Phys. C **17**, L233 (1984).

[28]The saturation intensity was estimated from the cross section computed in Sec. III B 4 and the value of $T_1 = 10$ ns from Ref. 29.

[29]H. R. Fetterman, Ph.D. thesis, Cornell University, 1968.

[30]M. Romagnoli, W. E. Moerner, F. M. Schellenberg, M. D. Levenson, and G. C. Bjorklund, J. Opt. Soc. Am. B **1**, 341 (1984).

[31]W. E. Moerner, M. Gehrtz, and A. L. Huston, J. Phys. Chem. **88**, 6459 (1984).

[32]W. von der Osten and W. Waidelich, Z. Phys. **178**, 244 (1964).

[33]A. Winnacker, R. M. Shelby, and R. M. Macfarlane, Opt. Lett. **10**, 350 (1985).

[34]H. W. H. Lee, M. Gehrtz, E. E. Marinero, and W. E. Moerner, Chem. Phys. Lett. **118**, 611 (1985).

[35]We presented a preliminary observation of this effect in Ref. 16.

[36]R. O. Pohl, in *Amorphous Solids: Low Temperature Properties,* edited by W. A. Phillips (Springer-Verlag, Berlin, 1981), pp. 27–64.

[37]W. Breinl, J. Friedrich, and D. Haarer, Chem. Phys. Lett. **106**, 487 (1984); W. Breinl, J. Friedrich, and D. Haarer, J. Chem. Phys. **81**, 3915 (1984).

[38]P. W. Anderson, B. I. Halperin, and C. M. Varma, Philos. Mag. **25**, 1 (1972).

[39]A recent publication has considered Gaussian distributions of asymmetries and splittings. See R. Jankowiak, R. Richert, and H. Bässler, J. Phys. Chem. **89**, 4569 (1985).

[40]J. Jäckle, Z. Phys. **257**, 212 (1972).

[41]R. T. Harley and R. M. Macfarlane, J. Phys. C **16**, 1507 (1983).

[42]J. A. Davis and D. B. Fitchen, Phys. Status Solidi B **43**, 327 (1971).

[43]G. Castro, R. H. Dicke, and D. Haarer, IBM Tech. Discl. Bull. **21**, 3333 (1979).

[44]G. C. Bjorklund and W. E. Moerner, IBM Tech. Discl. Bull. **26**, 5451 (1984).

[45]U. P. Wild, S. E. Bucher, and F. A. Burkhalter, Appl. Opt. **24**, 1526 (1985).

[46]U. Bogner, K. Beck, and M. Maier, Appl. Phys. Lett. **46**, 534 (1985).

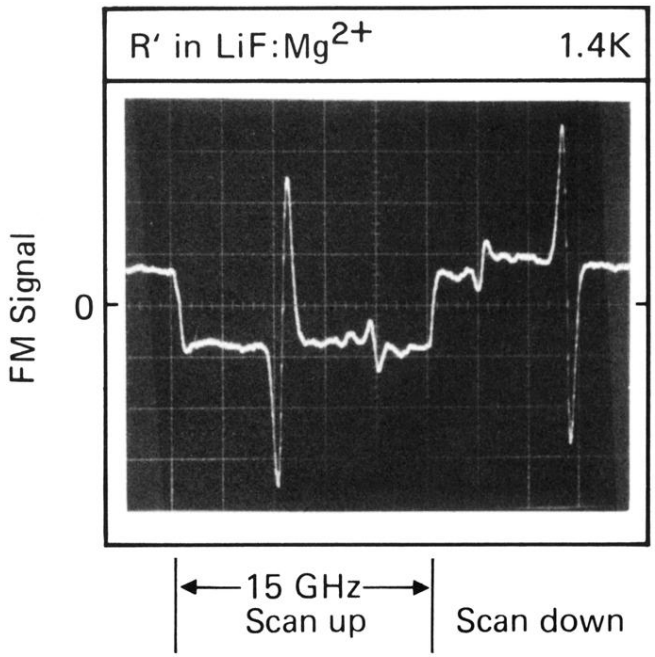

FIG. 7. FM signals resulting from PHB in LiF + 0.05 mol % MgF_2 at 1.4 K. The large signal results from reflection of the laser beam off a solid étalon before impinging on the detector. The laser frequency was held constant at the frequency corresponding to the center of the photograph for 30 s at a laser power of 10 mW to burn the hole shown. The scanning laser power was 10 μW in a 2-mm-diam spot, the burn wavelength was 8330.02 Å, and eight laser scans were averaged to produce the trace shown.

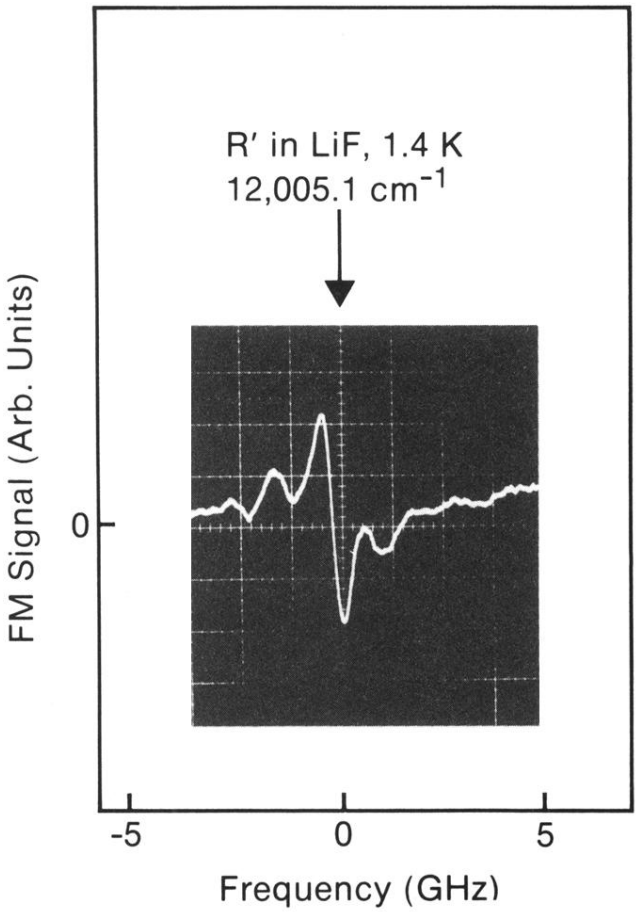

FIG. 8. FM spectrum of a single spectral hole burned in the R' center in LiF:Mg^{2+} ZPL origin absorption at 1.4 K. The burning and reading conditions are similar to Fig. 7, except that 64 scans were averaged to produce this trace.

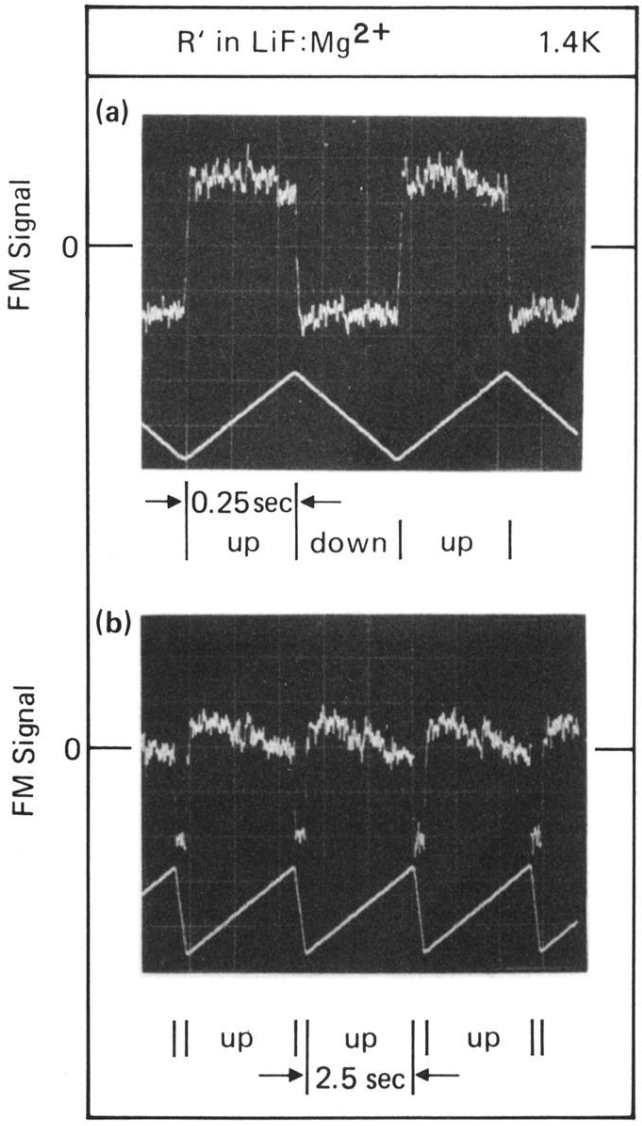

FIG. 9. Observation of transient hole-burning for R' centers in LiF:Mg^{2+} using laser FM spectroscopy. (a) The laser scan is symmetric, with 0.25 s for upward as well as downward scans. The laser scan covers a 15-GHz optical frequency range. The roles of positive and negative have been reversed compared to Fig. 7 using the phase shifter. The lower trace schematically depicts the instantaneous laser frequency. (b) Asymmetric laser scan: 2.5 s upward, 0.25 s downward. These traces were not averaged.